JPEDAV (2005) 26:311-321
DOI: 10.1361/154770205X56297
1547-7037/$19.00 ©ASM International

Modeling the Recrystallization Process Using Inverse Cellular Automata and Genetic Algorithms: Studies Using Differential Evolution

Tushar D. Rane, Rinku Dewri, Sudipto Ghosh, Kishalay Mitra, and N. Chakraborti

(Submitted July 5, 2004; in revised form April 15, 2005)

An inverse modeling approach was taken up in this work to model the process of recrystallization using cellular automata (CA). Using this method after formulating a CA model of recrystallization, differential evolution (DE), a real-coded variant of genetic algorithms, was used to search for the value of nucleation rate, providing an acceptable matching between the theoretical and experimentally observed values of fraction-recrystallized (X). Initially, the inverse modeling was attempted with a simple CA strategy, in which each of the CA cells had an equal probability of becoming nucleated. DE searched for the value of the nucleation rate yielding the best results for single-crystal iron at 550 °C. A good match could not be simultaneously achieved this way for the early stages of recrystallization as well as for the later stages. To overcome this difficulty, the CA grid was divided into two zones, having lower and higher probabilities of nucleation. This resulted in good correspondence between the predicted and experimental values of X for the entire duration of recrystallization. The introduction of a distribution in the probability of nucleation made the model even closer to the actual process, in which the probability of nucleation is often nonuniform due to nonuniformity in dislocation density as well as the presence of grain/interface boundaries.

1. Introduction

Thermomechanical processing of a material is carried out to tailor its microstructure and texture, which, in turn, helps to achieve the desired properties. Recrystallization is one of the mechanisms by which the microstructure and texture are altered during thermomechanical processing. It occurs by the nucleation and growth of dislocation-free grains within a region of high dislocation density.

Although studied by numerous researchers worldwide, there are still a number of issues related to the process of recrystallization that have defied precise analysis. For example, a reasonably accurate experimental determination of the nucleation rate and its mesoscopic distribution is not possible as the sizes of the critical nuclei are too small, and, although growing, they tend to merge with the other growing nuclei as well. The complexities associated with a theoretical evaluation of this parameter are also enormous. Thus, in a large number of recrystallization models that exist in the literature, the value of the nucleation rate, in most cases, has been arbitrarily chosen.[1-16]

In this study, we have used an evolutionary computing approach to circumvent the problem. At the core of our simulation runs a cellular automata (CA) scheme that is further augmented through the application of genetic algorithms (GAs), which provide the CA model with values of the model parameters, and also monitor its output. Genetic algorithms are biologically inspired computing techniques that come in many different forms.[17,18] What we have used here is known as differential evolution (DE).[19,20] Very limited work has been carried out utilizing GA within the CA framework.[21] It has not been done, so far, for modeling recrystallization or any other process involving a microstructural transformation. For further clarity about the adopted methodology, brief outlines of both CA and DE are provided below.

2. About Cellular Automata

CA[22–26] have been compared with a synthetic model of the universe in which the physical laws are expressed in terms of simple local rules in a discrete space-time structure. The efficacy of CA techniques lies in the fact that they can predict the behavior of a system at the macroscopic level when the rules governing the system at a microscopic level are known. They have already been used for modeling a large number of physical systems belonging to diverse disciplines like biology, chemistry, geology, and biochemistry.[22-26] In material science, the CA techniques are initially applied to problems related to solidification processes.[27,28] The methodology has been extended to phase transformation in subsequent studies, and recrystallization is one area that has been investigated in the process.[10-16]

As indicated before, CA deal with a discrete dynamic system,[22-26] the behavior of which is completely specified

Tushar D. Rane, the Department of Mechanical Engineering, Indian Institute of Technology Bombay, Powai, Mumbai 400 076, India; **Rinku Dewri,** the Department of Mathematics and Computing, and **Sudipto Ghosh** and **N. Chakraborti,** the Department of Metallurgical and Materials Engineering, Indian Institute of Technology, Kharagpur 721 302, India; and **Kishalay Mitra,** Manufacturing Industrial Practice, Tata Consultancy Service, 54B Hadapsar Industrial Estate, Pune 411 013, India. Contact e-mail: nchakrab@iitkgp.ac.in.

in terms of some local rules. To be more specific, CA deal with an array of cells the evolution of which is characterized by three features: the state of the cells; their neighborhood; and the rules for their transition. To construct any CA to simulate a specific problem, one needs to make a number of choices, the first being the selection of specific lattice geometry. Cellular automata require this lattice to be regular. In fact, it can be a linear (one-dimensional), triangular, square, hexagonal (two-dimensional [2-D]), or cubic (three-dimensional) array of cells. Once the lattice, *L*, is decided upon, we choose a neighborhood in which cells can interact. The neighborhood of a cell is described as a set of cells surrounding it. It is further elaborated in Fig. 1. For the nearest neighbors on a square lattice, the neighborhood, which is called the von-Neumann neighborhood of radius *r*, is described by:

$$N_{i,j} = \{(k,l) \in L : |k - i| + |l - j| \leq r\}$$

Another common neighborhood is the Moore neighborhood of radius *r*, defined as:

$$N_{i,j} = \{(k,l) \in L : |k - i| \leq r \text{ and } |l - j| \leq r\}$$

In the formal definition of CA, one usually requires the lattice to be infinite in all dimensions. For the considerations of computability and complexity, this is reasonable and necessary. However, it is difficult to simulate a truly infinite lattice on a computer, and therefore, one needs to prescribe some boundary conditions. Furthermore, the system that one wants to simulate may also require certain natural boundaries. Periodic, reflexive and fixed value boundaries are some of the options that are available in this scenario. This is elaborated in Fig. 2.

Along with the boundary conditions, the initial conditions are also required to start a CA simulation. In most cases the initial condition significantly influences the subsequent evolution. The initial conditions can be very specially constructed or, depending upon the nature of the problem, they can be randomly generated as well. One important consideration in the generation of initial conditions is that many CA rules conserve some quantities like the total number of particles, the total momentum, or energy and so on. Often some spurious quantities (i.e., quantities that are not conserved in the system to be modeled) can be conserved as well. In generating the initial conditions, care must be taken that the intended values of the conserved quantities are reached, especially when the random initial conditions are used, and that the spurious conserved quantities do not produce any undesired effects.

According to the definition of CA, each cell is a finite automaton, and therefore the set of states has a finite size. In addition, this set is usually kept fairly small because it simplifies the specification of rules, whereas a reason to use a large number of states can arise in some situations for better approximating a continuous system. A common construction of CAs is required to have several variables in each cell that must be stored in the state. In this case, we construct the state set *S* as the cross product of the sets for each variable. Formally, the state set is described as $S = U \times V$, where *U* and *V* are the set of values that the variables *u* and *v* can take. The size of the set *S* is $|S| = |U||V|$.

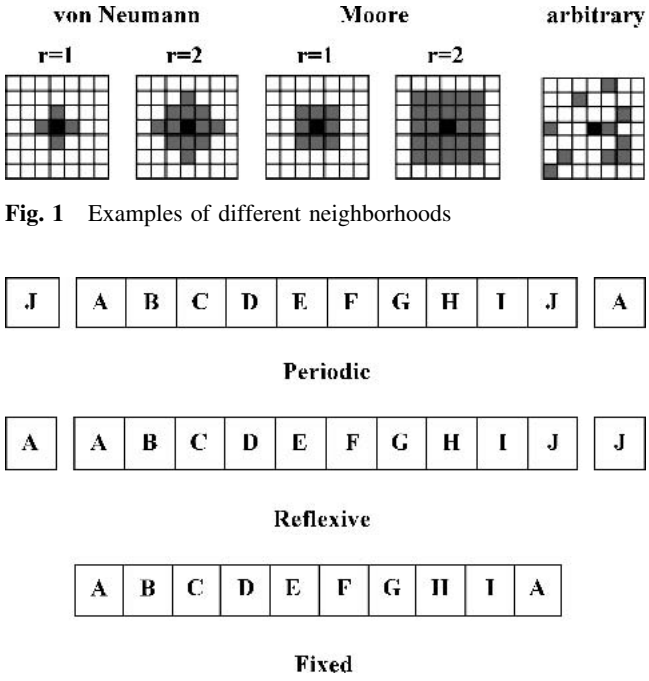

Fig. 1 Examples of different neighborhoods

Fig. 2 Different types of boundary condition

The most important aspect of CA is the transition rule or transition function. This is what affects the evolution most, and it depends on the lattice geometry, the neighborhood, and the state set. The transition rule determines how the state of a cell can change depending on the state of its neighbors. Rules can be directly specified by writing down the outcome of each possible configuration of states in the neighborhood. They can also be probabilistically specified where the outcome can be one of many states with associated probabilities. Formally, a transition rule can be expressed as:

$$T : S^n \times S \rightarrow s_P$$

where *S* and n are the state set and the number of cells in the neighborhood. s_P is a state from *S*, and it can occur with probability *P*. For direct specification of the rules, there will be only one state $s \in S$ with $P = 1$, and zero for the rest, for each possible configuration of the neighborhood. However, for probabilistic transition a positive value can be associated with one or more states in *S*.

In fact, CA can be considered an idealization of a physical system in which the space and time are discrete, and the physical quantities take only a finite set of values. In many real systems, the time evolutions of physical quantities are often governed by nonlinear partial differential equations. Owing to such nonlinearities, the solutions of these systems can often be very complex. Cellular automata provide an alternative approach for studying the behavior of such dynamic systems, subjecting them to an easier analysis by virtue of their inherent simplicity.

3. Basic Differential Evolution

The most common forms of GAs involve a binary encoding of the problem variables. An individual is formed by concatenation of the variables in their binary form. A randomly generated set of individuals constitutes the initial population containing a number of trial solutions. This population now evolves from generation to generation through some repeated, well-devised applications of the selection, crossover, and mutation operators, each devised analogously to their biological counterparts. Following a Darwinian framework, the individuals with higher fitness (i.e., the relatively better solutions) continue to emerge, survive, and reproduce until their ultimate convergence. Although highly robust and ubiquitous, the binary GAs are not devoid of problems. As discussed elsewhere,[18] they often require storage of very large binary arrays, in addition to repeated variable mapping between the binary and real space. Furthermore, in a situation known as Hamming cliff,[29,30] they become highly sluggish and often unsuitable for an essentially real variable problem. In DE, such difficulties are easily bypassed by doing away with binary representation altogether. A population of real-coded solution vector is allowed to evolve in DE, and both the crossover and mutation operations are conducted using a real-coded procedure. The crucial idea behind DE is to generate new trial variable vectors using direction information from the existing vectors.[19,20] The method is initiated by adding a weighted difference between two existing vectors to a third member, which essentially constitutes its mutation process. Through a specially designed crossover operation, the mutated vector is now recombined with a fourth member of the population to yield an offspring, and following a greedy strategy, the child replaces the parent if, and only if, it obtains a better fitness.

DE starts by randomly generating a population of real-coded solution vectors. For example, in the case of a four-variable problem, $\underline{X}_i = [x_1, x_2, x_3, x_4]$, will denote a typical solution vector in which the components x_1, x_2, x_3, and x_4 are the real-coded representation of the problem variables at a particular generation. A generation count G is maintained to keep track of the number of cycles completed during the evolutionary process. The initial population corresponds to generation $G = 0$.

Each of the members is then assigned a fitness value that represents how good the solution is in the problem domain. The concept of fitness here is essentially the same as that in the other forms of GAs. Next, for each vector $\underline{X}_{i,G}$, the corresponding mutated vectors are generated using three other randomly picked individuals such that:

$$\underline{V} = \underline{X}_{rl,G} + F.(\underline{X}_{r2,G} - \underline{X}_{r3,G})$$

where each one of $\underline{X}_{r1,G}$, $\underline{X}_{r2,G}$, and $\underline{X}_{r3,G}$ are randomly selected, but mutually different, vectors from the population. F is a real and constant factor that controls the amplification of the differential variation. The term $F(\underline{X}_{r2,G} - \underline{X}_{r3,G})$ determines the extent of the mutation of the vector $\underline{X}_{r1,G}$. The mutation here is self-adaptive in nature. For the initial generations, the population remains random, and, consequently, the differential term $(\underline{X}_{r2,G} - \underline{X}_{r3,G})$ remains large, resulting in a larger amount of mutation. As the population moves toward convergence, the system requires only a small amount of mutation, which is automatically achieved in DE because the differential term also tends to become small in such cases. Furthermore, by adjusting the parameter F, one can easily extend or contract the search domain. These are two additional advantageous features of DE that are normally not available in the binary coded GAs.

A specially designed crossover operator now takes over to introduce diversity into the new parameter vector $\underline{V}$. It involves probabilistically replacing a few elements of the vector with original values from $\underline{X}_{i,G}$, to form the final trial vector $\underline{U}$:

$$\begin{aligned} u_j &= y_j, \quad \text{if } r_j \le P_{cr} \\ &= x_i, \quad \text{if } r_j > P_{cr} \end{aligned}$$

where x_j belongs to $\underline{X}_{i,G}$, r_j is a random number, P_{cr} is the crossover probability, and u_i and v_i denote the typical components of the vectors $\underline{U}$ and $\underline{V}$. Additionally, it is always ensured that $\underline{U}$ is able to retain at least one component of the mutated vector $\underline{V}$. A fitness value is computed for this trial vector as well.

A comparison of the fitness values is now made between the parent $\underline{X}_{i,G}$ and the child $\underline{U}$, and the one having better fitness is passed on to the next generation as $\underline{X}_{i,G+1}$. This completes one generation of the evolutionary process, and the whole process is repeated with this newly generated population. The same procedure continues until the solution vectors converge.

The basic operations involved in DE are shown schematically in Fig. 3 for an arbitrary variable problem.

4. Modeling the Recrystallization Process

Models of recrystallization can be divided into two broad classes: analytical and probabilistic. Analytical models are based on Johnson-Mehl-Avrami-Kolmogorov relationship.

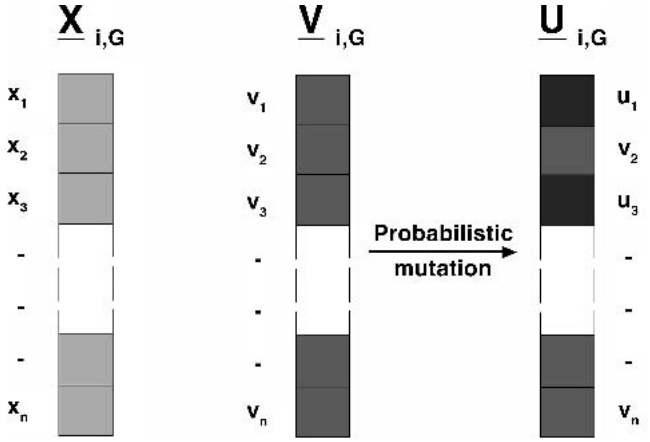

Fig. 3 Mutation and crossover operations in DE

Monte-Carlo and CA models are probabilistic approaches. A CA model of recrystallization has certain advantages over other models. One of the important advantages of a CA simulation is that it can be directly related to the evolution of microstructure and features like the spatial distribution of a second phase can be demonstrated convincingly.

Cellular automata models have been successfully used in predicting the variation of fraction-transformed (X) as a function of time during recrystallization.[10-16] The rate of nucleation is one of the parameters in the CA models. However, as indicated before, a reasonably accurate estimation of the rate of nucleation is not possible because of several constraints. Thus, an evolutionary inverse CA modeling was undertaken in this study to estimate the nucleation rate and the mesoscopic distribution of recrystallization probability on the basis of the available experimental data concerning the variation of X with time. The objective of inverse modeling is to estimate the input parameter settings for which the model prediction closely matches the corresponding experimental results. Therefore, it is essentially a problem of optimization in which we search for the parameter settings that would result in a minimum deviation of the model prediction. Thus, in this case, the set of parameters constitutes the variable vector used in the optimization scheme. Because the search space for the CA parameters is quite wide, the need for a heuristic approach was automatically felt. The method of DE was used to find the right choice of the parameter vector that would minimize an error function. On an industrial scale, the parameters obtained by inverse calculation can be used for the prediction of X and also the spatial distribution of the recrystallized zones as a function of time. This basic methodology is further elaborated below.

4.1 The Implementation of Cellular Automata

In the present work, the CA represent a small portion of the 2-D cross section of the material undergoing recrystallization, and it is composed of a 2-D array of cells. The 2-D array consists of a total of 10^6 cells to represent an area of 0.25 cm^2. Thus, δ_{cell}, the length (or breadth) of each cell, is equal to 5 μm, providing enough accuracy to the model. Each of the squares can be in one of the two states: recrystallized or un-recrystallized. Initially (i.e., at time = 0), all of the cells are in an un-recrystallized state. In each subsequent time step, few cells are transformed into the recrystallized state from their un-recrystallized state. The CA model predicts the distribution of the recrystallized region at different time steps by adopting the following strategy.

Transformation of an unrecrystallized cell to a recrystallized one, with the increment in the time step, occurs in two different ways in our model. Few cells are randomly chosen and transformed into recrystallized cells, if they are found to be unrecrystallized. Physically, this simulates the process of nucleation. Thus, each unrecrystallized cell has a probability of nucleation, which is given by the number of nucleation events for each time step increment ($\mathbf{n_r}$) divided by the total number of cells.

The second way in which the transformation of the cells occurs is by the growth of the recrystallized region in the CA, which simulates the growth phenomenon of the recrystallized zone in a real material. During this process, the unrecrystallized cells within a neighborhood of recrystallized cells transit to the recrystallized state. Because the neighborhood can be of many different types, its proper description warrants further clarification. In the present work, each cell in the recrystallization CA model is assumed to be associated with an extended Moore neighborhood, as shown in Fig. 4. The extended Moore neighborhood consists of 24 cells around the central cell as shown in Fig. 4. This neighborhood was chosen to incorporate the slowing down of the growth process, as has been done by Hesselbarth and Gobel.[10] This will be explained later.

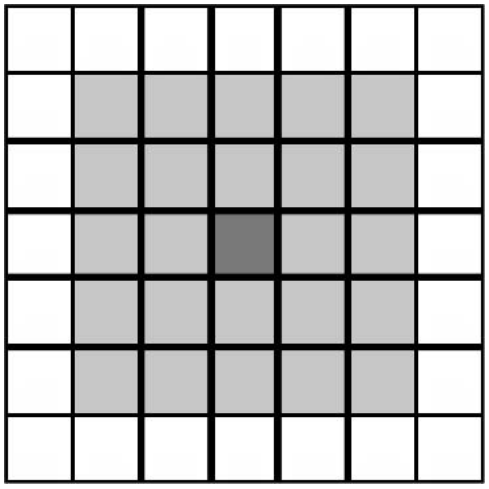

Fig. 4 The extended Moore neighborhood

For defining the neighborhood of the boundary cells, a periodic boundary condition was assumed.

Because there were only two possible states of a cell in the CA (i.e., recrystallized or unrecrystallized), we used logical arrays instead of integer arrays to represent the cellular arrangement, reducing the runtime memory usage in the process. Also, instead of copying the new cell states to the arrays having old cell states, we switched the pointers to these two arrays to save the computing time.

The CA model predicts the spatial distribution of recrystallized zones at integral time steps. One needs to estimate the real (physical) time corresponding to the integral time steps. In each time interval, a recrystallized region advances by two cells (i.e., a distance of 2 δ_{cell}), which is equal to 10 μm in the current study. The recrystallized region advances $2\delta_{cell}$ with a speed of growth rate (G). Thus, the real time interval (Δt_{real}) between two consecutive time step will be given by:

$$\Delta t_{real} = \frac{2 \times \delta_{cell}}{G} \qquad \text{(Eq 1)}$$

Here, we have used the recrystallization data for single-crystal iron at 550 °C, for which the Cahn-Hagel growth velocity relation[31] is expressed as:

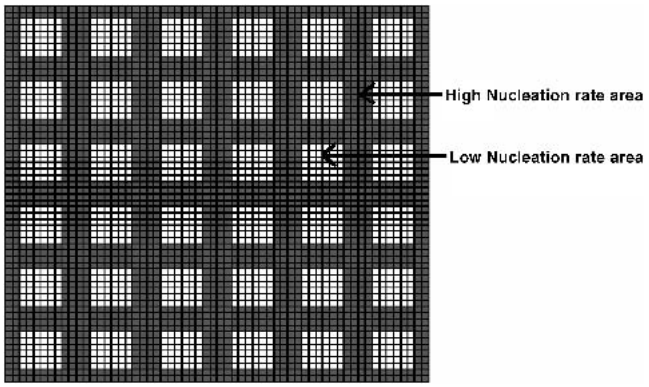

Fig. 5 Zones of low and high nucleation

$$G = 26.45\ t^{-0.38}\ \mu\text{m/min} \qquad \text{(Eq 2)}$$

In some alloys, it has been observed that the rate of recrystallization slows down in its final stage. To incorporate this effect into the model, we have used the concept of impeded impingement of grains that was introduced earlier by Hesselbarth and Gobel.[10] To simulate the impeded impingement in the CA model, Hesselbarth and Gobel[10] assigned a lower (<1.0) probability of transition (P_t) to the cells, when the number of recrystallized cells in their extended Moore neighborhood exceeded 11. The same approach was adopted in the current study.

However, few simplifying assumptions regarding the growth of nuclei are made in our model. We have considered the rate of growth to be the same in two perpendicular directions, which may not be strictly valid in a real situation. Second, we have not taken into account the fact that during recrystallization different nuclei may have different growth rates due to differences in their crystallographic orientations with respect to the parent grains.

Because the probability of nucleation will not be uniform in the mesoscopic scale, owing to the nonuniformity in dislocation density, here, following the approach of Hesselbarth and Gobel,[10] we have considered two types of zones, having high and low recrystallization probabilities. Considering a simple periodic spatial distribution of the zones of high probability, the entire problem domain is divided into equal-sized squares, as shown in Fig. 5. In each square, the zone of high probability is located within a band adjacent to the square boundary.

After considering the spatial distribution of nucleation probability at mesoscopic scale, we have come up with a total of five parameters for the CA model, which are listed below:

- Nucleation rate in the CA array (n_r)
- Transition probability (P_t)
- Square size or the periodicity of the spatial distribution of the high-probability band (S)
- Area fraction of the high-probability band within each square (α)
- The ratio of probability in the high-probability band to that in the low-probability zone (ρ_{ratio})

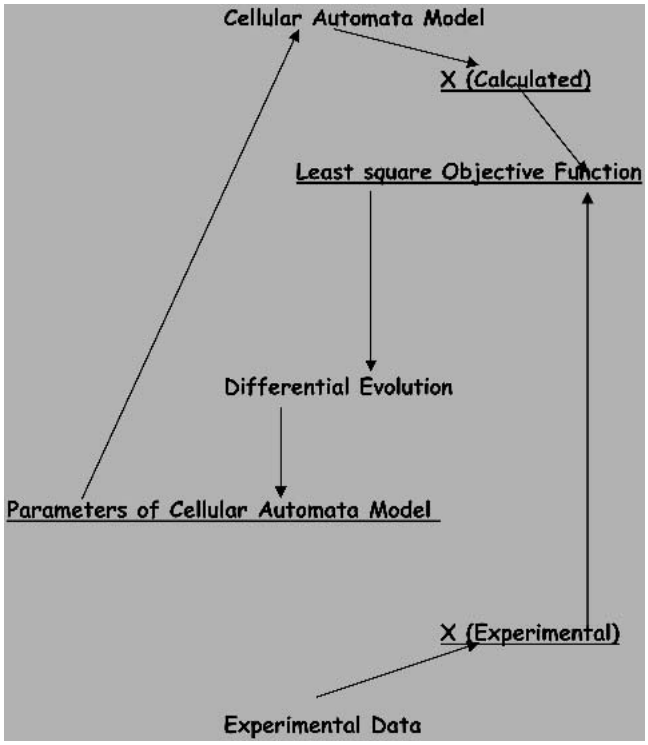

Fig. 6 Schematics of computing strategy

4.2 Evolutionary Inverse Approach for Estimation of Nucleation Rate and Its Mesoscopic Distribution

Each of these parameters is fuzzy and is estimated through an inverse calculation using DE. The CA model took the fuzzy parameters, which were also the decision variables in DE, as input and predicted X. A match between the X values calculated using the CA model and those obtained experimentally was sought. This was obtained through DE by minimizing the least-squares error between the two quantities, and the whole procedure was repeated until the emergence of an optimum set of parameters.

$$\text{Fitness function} = \Sigma\ (\text{predicted X} - \text{experimental X})^2$$

It should be noted at this point that a CA model would deal only with discrete time steps. Therefore, X values could not be calculated at some intermediate time steps where the experimental data were available. A linear interpolation method was used to compute X in such cases.

The computing procedure is schematically illustrated in Fig. 6.

We have attempted to adopt this procedure for five CA models having different combinations of the model parameters listed in the previous section. Further details are provided in the subsequent section. For all cases, a population size of 30 and a generation count of 50 were used in searching for the values of the model parameters that would result in the best fit with the available data on the variation of X with time.[5] The mutation constant F was taken as 0.8, and P_{cr} was taken as 0.5. Convergence was ensured by making

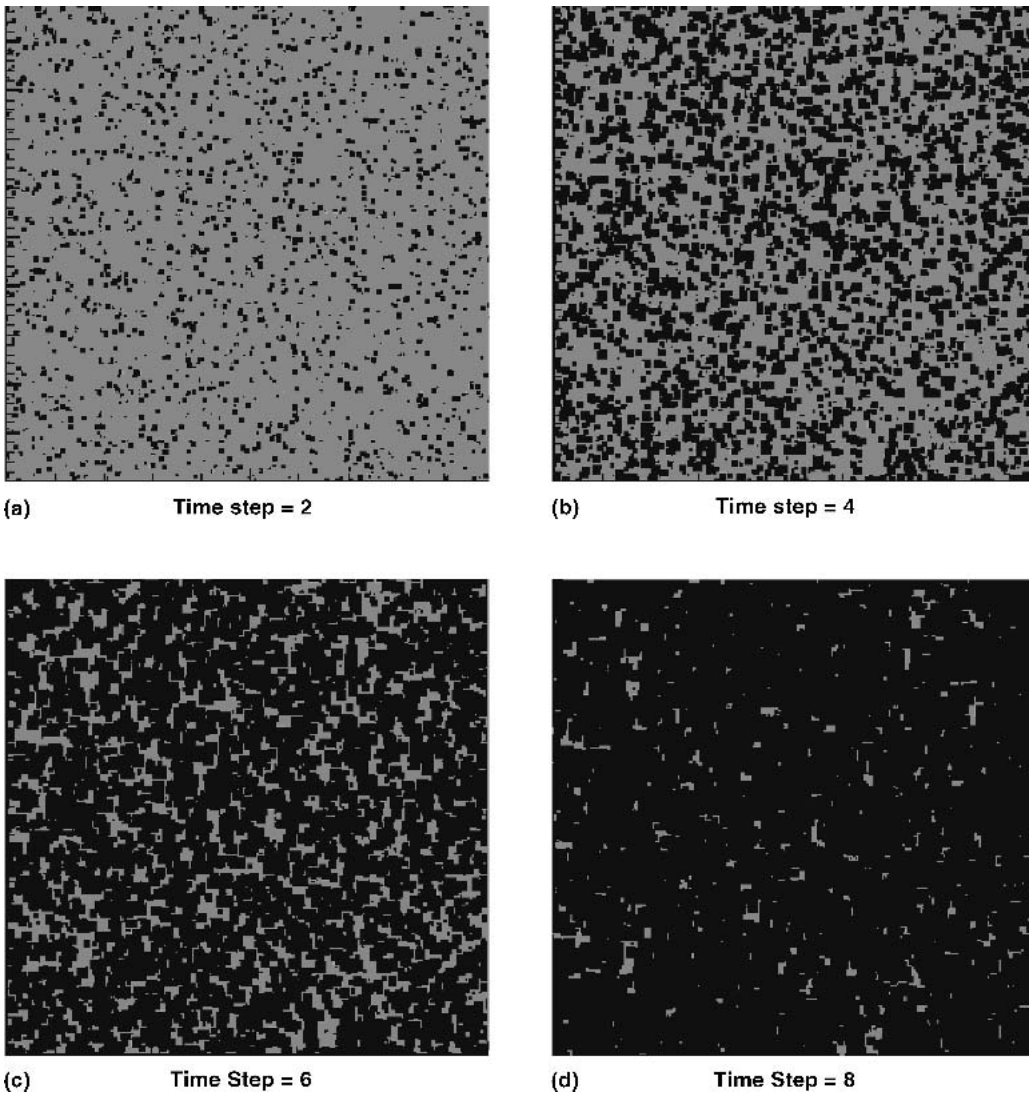

Fig. 7 Evolution of the CA array at different time steps ($n_r = 849$). Light zone, unrecrystallized; dark zone, recrystallized

the maximum, minimum, and average fitness values fall within a narrow interval, and no further improvement of fitness was possible with enhanced mutation.

5. Results of Inverse Modeling

As mentioned before, the inverse CA modeling was accomplished using five progressively complex CA models. In the first and simplest CA model, nucleation was randomly seeded in the 2-D array, and thus all cells had an equal probability of becoming nucleated. A simple growth rule (i.e., a cell is recrystallized in the next time step if it finds at least one recrystallized cell in its neighborhood) was imposed. Figure 7 shows the evolution of the microstructure at different time steps in this case. The inverse modeling using the first model thus involved only one decision variable (i.e., the nucleation rate [n_r]).

In this search, n_r varied from 1 to 100,000. The best-fitting variation of X with time, obtained from this model, is shown in Fig. 8, along with the experimental data points. The nucleation rate corresponding to the best-fit curve was 849 cells per time step. The fit appears to be reasonable only for time >60 s.

For the early stage of recrystallization (time <60 s), the percentage deviation of the predicted X values from the experimental data was high. DE however, is a sufficiently robust method for searching the optimum parameter settings that would provide the best fit. Therefore, the failure to obtain a good match, both in the beginning and at the later stages of recrystallization, is due to the inherent limitations of this simplistic CA model, and not to any shortcomings of the DE technique.

Higher nucleation rates would provide a better fit for time $t < 60$ s. However, this will also disturb the good match obtained for $t > 100$ s (which was obtained for $n_r = 849$) because the predicted value of X would be higher than the experimentally observed values. It appeared that a combi-

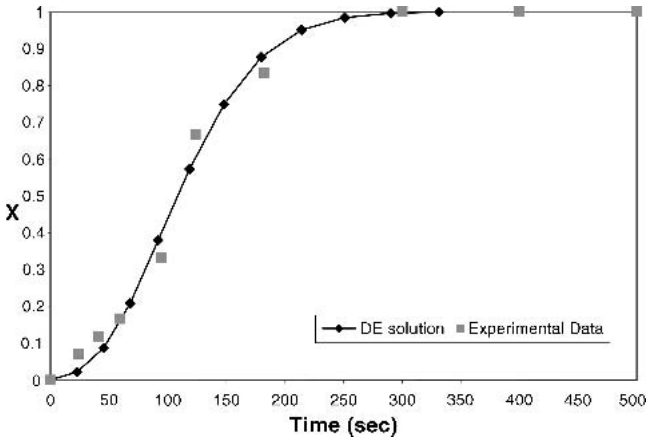

Fig. 8 DE solution versus experimental data (decision variable n_r)

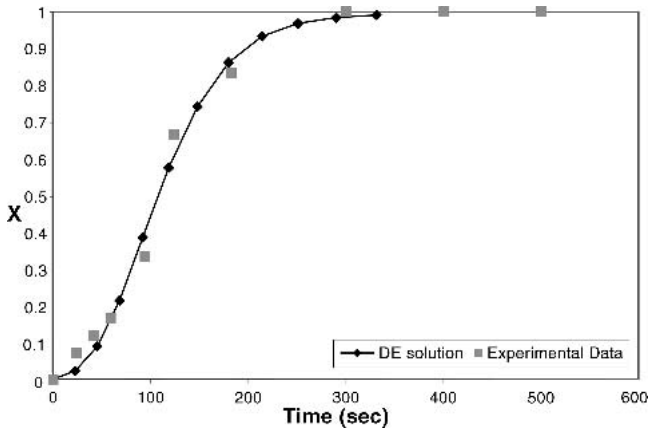

Fig. 9 DE solution versus experimental data (decision variables n_r and P_t)

nation of higher nucleation rate and the impeded impingement rule, which reduces the rate of recrystallization at a later stage, would provide a better fit with the experimental data available for $t < 60$ s, and also at the later stage of recrystallization. Therefore, the CA model was enhanced by assigning transition probability (P_t) to the cells having more than 11 recrystallized cells in their extended neighborhoods. P_t varied from 0.0 to 1.0. However, no combination of n_r and P_t could provide a good fit for time less than ~60 s and simultaneously at the later stage of recrystallization. This is evident by comparing Fig. 8 and 9. For the second model, as in the first, the percentage error has been found to be high for a time less than ~60 s. Thus, the incorporation of the impeded impingement rule really did not constitute a very significant improvement.

In the third model, the CA analysis was further enhanced by incorporating the distribution of nucleation probability, as discussed earlier, and the transition probability was frozen to 1.0 (i.e., the impeded impingement rule was not applied). Here the decision variables were n_r, S, and α. During the simulation, n_r was varied from 25 to 110,889,000, S was varied from 3 to 200, and α was varied between 0.1 and 0.33. Figure 10 shows the evolution of the CA arrays at different time steps for this case. In this case, the quality of the fit has improved significantly, as can be seen from Fig. 11, especially for times less than ~60 s. Thus, considering the spatial distribution, it is possible to obtain a good fit for times less than ~60 s, as well as for the higher times.

In the fourth model, in addition to the variables considered in the third case, P_t was introduced as a decision variable. The value of P_t was varied from 0 to 1. This exercise did not show any improvements in the fit, again suggesting that P_t is not an important parameter in the model (Fig. 12).

Finally, in the fifth model, in addition to the third case, ρ_{ratio} was introduced as a decision variable. The value of ρ_{ratio} was varied from 0.1 to 0.33. The best fit obtained in this case is shown in Fig. 13.

The optimum values of the parameters found by DE for each of the five models discussed above are shown in Table 1.

The statistical analysis included in the Appendix would provide some further insight on the trends of the results.

6. Discussion

The CA models of recrystallization developed during this study have several advantages over the more traditional models. One important advantage is that the CA simulation can be directly related to the evolution of microstructure. Any CA model is based upon the idea that the evolution of a cell is dependent on the evolution of its neighboring cells, which in turn, depends on the evolution of the cells in their respective neighborhoods. Thus, the evolution of any particular cell is dependent on the evolution of the rest of the cells in the CA. Therefore, the spatial distribution of the state of the cells in the automata must necessarily influence the evolution of a particular cell. In this way, a CA-based recrystallization model closely mimics the actual process that it attempts to emulate.

Like any other models of recrystallization, CA models would also require the rates of nucleation and growth for predicting the evolution of the microstructure. However, as stated earlier, so far it has not been possible to estimate the precise value of the nucleation rate, either through experimental or theoretical procedures. As elaborated here for single-crystal Fe, a CA-based procedure can overcome this difficulty through inverse modeling. Due to this unique attribute, a hybrid CA procedure like the one adopted here becomes highly effective for the estimation of the rate of nucleation and also its mesoscopic distribution, provided that the growth rate or the migration velocity is known.

It is evident from the results presented in the previous section that the CA models that assume uniform nucleation probability throughout the cross section have some inherent limitations. Such models, as observed in this study, could not be used for simultaneously simulating the early and later stages of recrystallization. Even a robust search technique like DE could provide very little help in improving the situation, when such models are used. As per Fig. 8 and 9, the first two CA models with the best possible value for n_r and P_t tend to underpredict the values of X in the early part of recrystallization. Similar trends were also noted in the earlier CA models of recrystallization,[13,16] which also assumed a uniform nucleation rate.

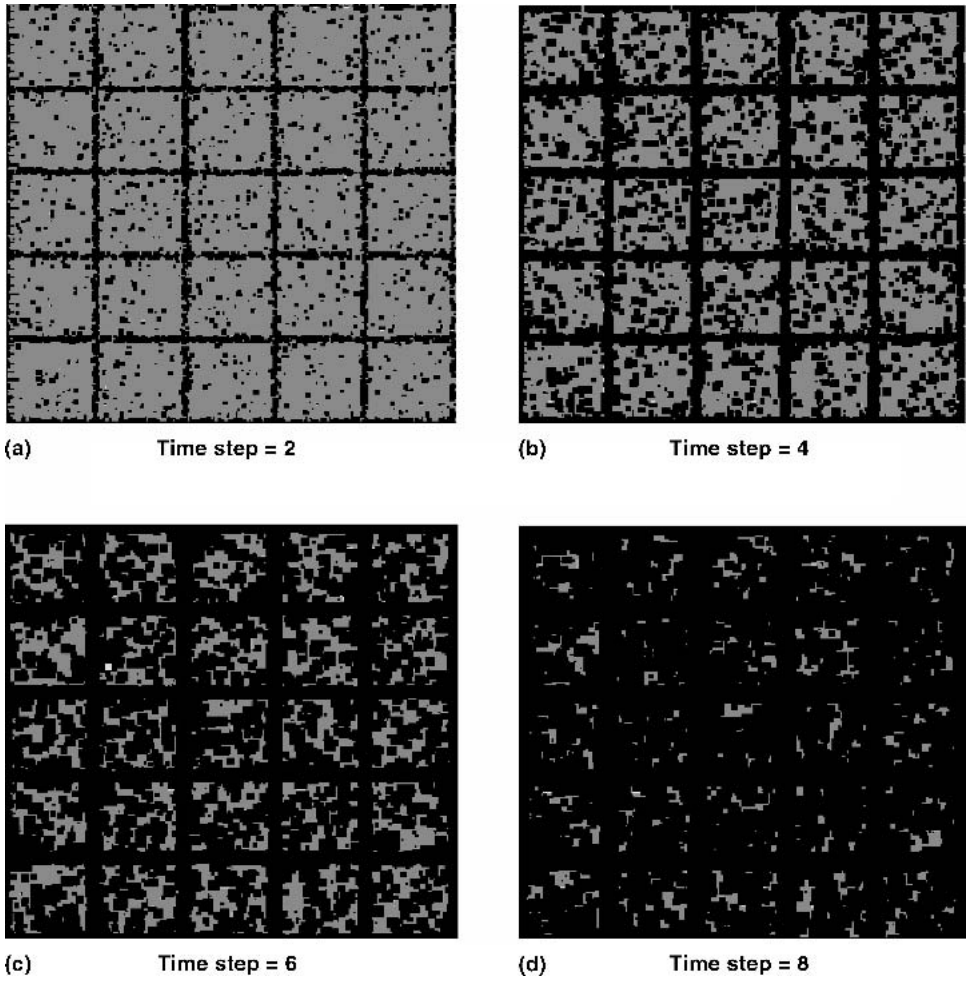

Fig. 10 Evolution of the cellular automaton array at different time steps ($n_r = 2500$, $S = 195$, and $\alpha = 0.1$) Light zone, unrecrystallized; dark zone, recrystallized

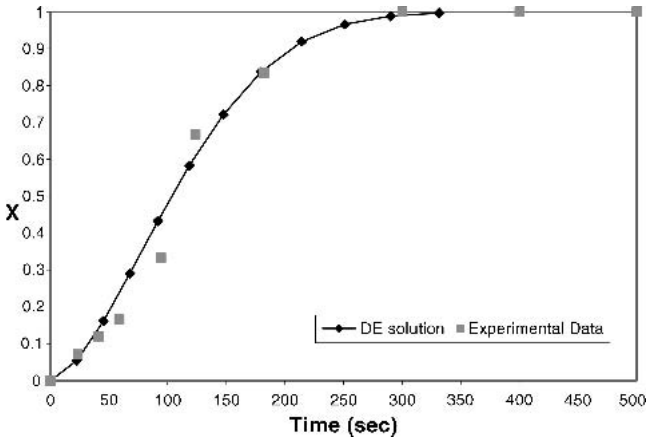

Fig. 11 DE solution versus experimental data (decision variables, n_r, S, and α)

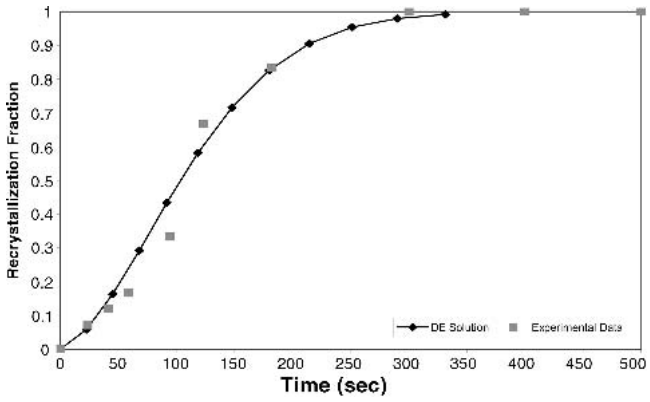

Fig. 12 DE solution versus experimental data (decision variables n_r, S, α, and P_t)

Incorporating the distribution of the nucleation probability over the CA grid divides recrystallization in two stages. During the early stage of recrystallization, the kinetic process is dominated by the transformation in the high-probability zone, which practically is over within a short period of time (Fig. 10). In the later stage, the transformation in the low-probability zone dominates the kinetics, as the high-probability zone attains its saturation by then. The results of the third, fourth, and fifth CA models have indi-

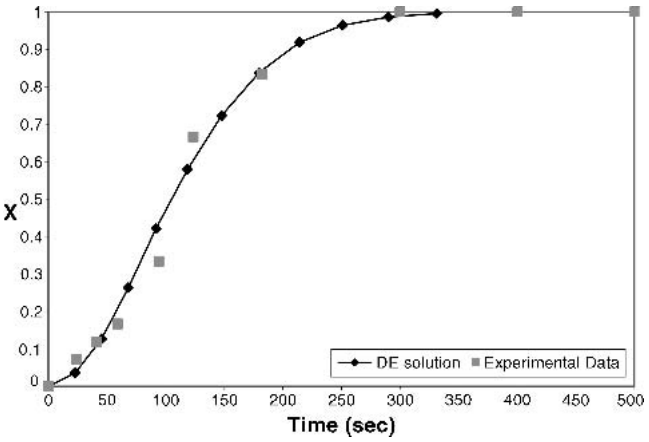

Fig. 13 DE solution versus experimental data (decision variables n_r, S, α, and ρ_{ratio})

Table 1 The optimum parameters determined by DE

Model No.	Optimum parameter values
1	n_r: 849 nuclei/time step
2	n_r: 849 nuclei/time step
	P_t: 0.405
3	n_r: 2500 nuclei/time step
	S: 195 cells × 195 cells
	α: 0.1 ($P_t = 1$)
4	n_r: 2736 nuclei/time step
	S: 171 cells × 171 cells
	α: 0.1
	P_t: 0.589
5	n_r: 1449 nuclei/time step
	S: 163 cells × 163 cells
	α: 0.146
	ρ_{ratio}: 0.33

cated that, apart from the fraction of the high-probability zone, its spatial distribution also influences the kinetics of transformation (i.e., the variation of X with time). In this investigation, a periodicity of 163 to 195 cells gave the best fit with the experimental data points.

It is important to note that in the present state of model development, it may not always be possible to differentiate between the performances of CA models 3, 4, and 5. Any further enhancement in this direction would require detailed experimental data, such as the size distribution of the recrystallized zones, texture distribution, initial grain size, and dislocation density distribution, which are unavailable at the moment. Thus, presently we can make only a rough estimate of the rate of nucleation, which varies from ~1500 to ~2700 nuclei per unit time-step per 0.25 cm^2. The spread is substantially less compared to the earlier theoretical estimates, which often varied by four orders of magnitude.[31] It should be noted that an enhancement of the CA model based on the experimental data on grain size and the distribution of dislocation density (which can be estimated from the microhardness variation) can further reduce the uncertainty level.

It needs to be pointed out at this stage that the phenomenological model provided here for the heterogeneous nucleation does not explicitly refer to the cellular structure of the dislocations observed in the heavily deformed metals. This was done to retain the inherent simplicity of the approach that we took, and not to burden it further with additional details that would certainly involve the engagement of a few more uncertain parameters. It is well known that the strain energy associated with the dislocation structure in a deformed metal is actually the repertoire of the driving force needed for the nucleation to occur. Also, in a cellular structure of dislocations, the probability of nucleation inside the cell would be quite negligible. The regions of high nucleation density that we have considered here should be interpreted as grain boundaries having larger length scales and providing heterogeneous nucleation sites, rather than as dislocation cellular structures, although the driving force is still provided by the dislocation network. Any question of transformation within a subgrain does not arise in such a scenario. Realistically, the dislocation configurations in the deformed regions are far from being ordered. Owing to the deviation from an ordered structure, local fluctuations exist in the strain-energy distribution, and their peak values enable nucleation to occur by overcoming an Arrhenius-type activation energy barrier. This, in turn, tends to drive the local energies of these regions more toward a thermodynamic equilibrium, thus, progressively eliminating them as a source of future nucleation. Such details on the microscale would be absolutely essential for constructing a system model requiring a closed-form solution of every system equation. However, one can afford not to use such information directly in the inverse-modeling approach that we have adopted here, as it can capture the essentials at a macroscopic level following a path laid out by the existing experimental data.

Apart from developing an inverse CA model using DE that provides a reasonable estimate of the rate of nucleation, the present work brings out the importance of mesoscopic heterogeneity (i.e., spatial distribution on a mesoscopic scale) in the CA modeling of recrystallization. The incorporation of mesoscopic heterogeneity also brings the model closer to the physics of the actual process. During the stage of cold-working or plastic deformation, the deformation and dislocation density, as indicated earlier, are not uniform. This leads to nonuniformity in the rate of nucleation as well. Also, the rate of heterogeneous nucleation at the grain boundary is expected to be higher, further justifying the need for incorporating the mesoscopic heterogeneity.

7. Conclusions

This study has elaborated several advantages of CA models of recrystallization over the more conventional alternatives. A CA simulation can be directly related to the evolution of microstructure, which can be considered to be a prime advantage. Due to experimental as well as theoretical limitations, it is not possible to directly obtain a reasonable estimate of the rate of nucleation and its mesoscopic distribution. The CA models of recrystallization that have been developed so far have used some arbitrarily chosen

value of nucleation rate and its distribution. The inverse-modeling approach taken up in this work could overcome this limitation. The CA model used in the present scheme is augmented through a real-coded variant of GAs that provided the CA model with values of the model parameters and also monitored its performance by evaluating a fitness function. Inverse modeling revealed the necessity of incorporating a mesoscopic distribution of the nucleation sites into the CA model, predicted some acceptable microstructures, and also predicted the nucleation rates within a lower amount of uncertainty than that currently existing in the literature.

Finally, GAs are suitable for problems of very high complexity,[32] and they are gradually becoming ubiquitous in the field of materials[33]; however, the obvious advantage of coupling them with a powerful evolutionary algorithm like cellular automation is yet to be fully exploited by the researchers in this area. Furthermore, GAs are now making their presence felt in the simulation of the industrial rolling processes,[34,35] in which studies such as the present investigation can indeed make a substantial contribution.

Acknowledgment

Useful pointers from an anonymous reviewer regarding the role played by the cellular dislocations and strain energy are thankfully acknowledged.

Appendix: Statistical Analysis

The correlation coefficient gives us a measure of how well the predicted values from a simulation model fits the experimental data. The strength of the relationship between the two data sets is characterized by a numerical value between 0 and 1; the better the correlation, the higher the number. The Pearson product moment correlation uses variance and covariance measures to determine this estimate of the relationship. Given two data sets, X and Y, with cardinality N, the Pearson correlation is given by the following.

$$r = \frac{\sum XY - \frac{\sum X \sum Y}{N}}{\sqrt{\left[\sum X^2 - \frac{(\sum X)^2}{N}\right]\left[\sum Y^2 - \frac{(\sum Y)^2}{N}\right]}}$$

Table A-1 lists the Pearson correlation and the RMS error obtained from the five different variants of the CA model used in this study. The high correlation coefficient values show that all of the models perform well in predicting the dependent variable. Errors in models 1 and 2 are comparatively lower than those in the other three models.

However, the predicted curves in models 1 and 2 show more deviation in the initial part of the time-scale (<60 s) than the other three models. The faster growth of the experimental values in this time interval is better accommodated in model 5. Hence, we divided the entire time-scale into three different parts (0 to 60 s, 60 to 150 s, and >150 s), and individual RMS errors in each of these intervals were calculated. Note that the experimental data show a high gradient shift in its trend at the adjoining points of these time intervals. A histogram of the calculated errors for models 1, 2, and 5 is shown in Fig. A-1. We found that model 5 gives a better prediction during the time intervals 0 to 60 s and >150 s, but shows some divergence in the intermediate areas. The average error from these three intervals is, however, least in the case of model 5.

Table A-1 Correlation coefficient and RMS errors

Model	*r*	RMS error
1	0.9928	0.0459
2	0.9927	0.0446
3	0.9890	0.0566
4	0.9889	0.0576
5	0.9898	0.0498

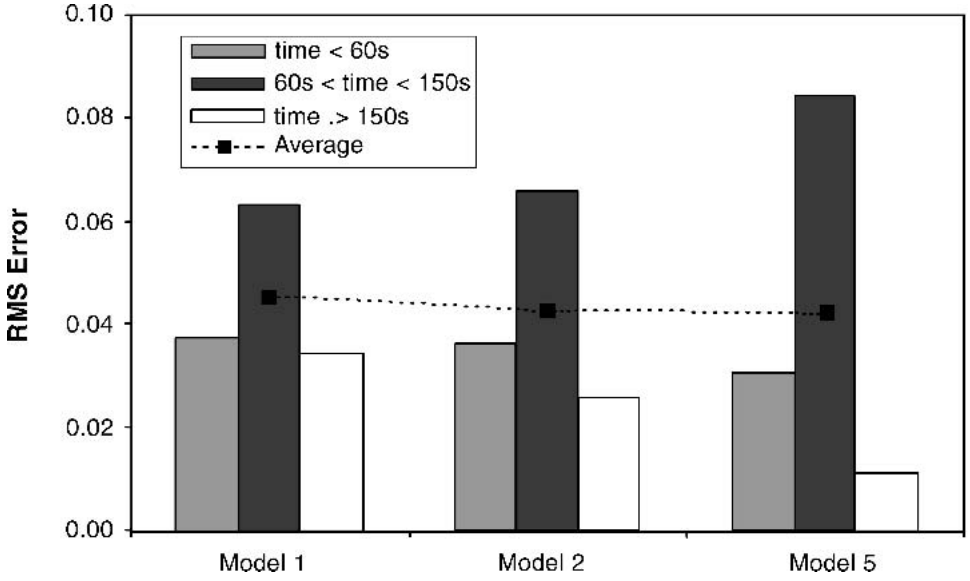

Fig. A-1 Histogram showing error estimates from the three better performing models

References

1. K.W. Mahin, K. Hanson, and J.W. Morris, Comparative-Analysis of the Cellular and Johnson-Mehl Microstructures Through Computer-Simulation, *Acta Metall.,* Vol 28, 1980, p 443-453
2. D.J. Srolovitz, G.A. Grest, and M.P. Anderson, Computer-Simulation of Recrystallization: 1. Homogeneous Nucleation and Growth, *Acta Metall.,* Vol 34, 1986, p 1833-1845
3. D.J. Srolovitz, G.A. Grest, M.P. Anderson, and A.D. Rollett, Computer-Simulation of Recrystallization: 2. Heterogeneous Nucleation and Growth. *Acta Metall.,* Vol 36, 1989, p 2115-2128
4. K. Marthinsen, O. Lohne, and E. Nes, The Development of Recrystallization Microstructures Studied Experimentally and by Computer-Simulation, *Acta Metall.,* Vol 37, 1989, p 135-145
5. R.A. Vandermeer and B.B. Rath, Modeling Recrystallization Kinetics in a Deformed Iron Single-Crystal, *Metall. Trans.,* Vol 20A, 1989, p 391-401
6. H.E. Vatne, T. Furu, R. Orsund, and E. Nes, Modelling Recrystallization After Hot Deformation of Aluminum, *Acta Mater.,* Vol 44 (No. 11), 1996, p 4463-4473
7. D. Juul Jensen, Modeling of Microstructure Development During Recrystallization *Scr. Metall. Mater.,* Vol 27, 1992, p 1551-1556
8. E. Woldt, New Kinetic Model for Primary Recrystallization of Pure Metals, *Metall. Mater. Trans. A,* Vol 32, 2001, p 2465-2473
9. A.T.W. Kempen, F. Sommer, and E.J. Mittemeijer, Determination and Interpretation of Isothermal and Non-Isothermal Transformation Kinetics: The Effective Activation Energies in Terms of Nucleation and Growth, *J. Mater. Sci.,* Vol 37, 2002, p 1321-1322
10. H.W. Hesselbarth and I.R. Gobel, Simulation of Recrystallization by Cellular Automata, *Acta Metall.,* Vol 39, 1991, p 2135-2143
11. C.F. Pezzee and D.C. Dunand, The Impingement Effect of an Inert, Immobile 2nd Phase on the Recrystallization of a Matrix, *Acta Metall. Mater.,* Vol 42, 1994, p 1509-1524
12. C.H.J. Davies, The Effect of Neighborhood on the Kinetics of a Cellular-Automaton Recrystallization Model, *Scr. Mater.,* Vol 33, 1995, p 1139-1143
13. C.H.J. Davies, Growth of Nuclei in a Cellular Automaton Simulation of Recrystallisation, *Scripta Mater.,* Vol 36, 1997, p 35-40
14. R.L. Goetz and V. Seetharaman, Static Recrystallization Kinetics With Homogeneous and Heterogeneous Nucleation Using a Cellular Automata Model, *Metall. Mater. Trans.,* Vol 29, 1998, p 2307-2321
15. R.L. Goetz and V.Seetharaman, Modeling Dynamic Recrystallization Using Cellular Automata, *Scr. Mater.,* Vol 38, 1998, p 405-413
16. C. H. J. Davies and L. Hong, The Cellular Automaton Simulation of Static Recrystallization in Cold-Rolled AA1050, *Scr. Mater.,* Vol 40, 1999, p 1145-1150
17. Z. Michalewicz, *Genetic Algorithms + Data Structures = Evolution Programs,* Springer-Verlag, Berlin, 1999
18. N. Chakraborti, Genetic Algorithms in Ferrous Production Metallurgy, *Surveys Math. Indust.,* Vol 10, 2002, p 269-291
19. K. Price and R. Storn, Differential Evolution, *Dr. Dobbs J.,* Vol 22, 1997, p 18
20. N. Chakraborti and A. Kumar, The Optimal Scheduling of a Reversing Strip Mill: Studies Using Multipopulation Genetic Algorithms and Differential Evolution, *Mater. Manufact. Proc.,* Vol 18, 2003, p 433-445
21. M. Mitchell, J.P. Crutchfield, and R. Das, Evolving Cellular Automata to Perform Computations, *Handbook of Evolutionary Computation,* T. Back, D.B. Fogel, and Z. Michalewicz, Ed., Institute of Physics Publishing, Bristol, and Oxford University Press, Oxford, 1997
22. S. Wolfram, *Theory and Applications of Cellular Automata,* World Scientific, Singapore, 1986
23. A. Ilachinski, *Cellular Automata: A Discrete Universe,* World Scientific, Singapore, 2001
24. T. Toffoli and N. Margolus, *Cellular Automata Machines: A New Environment for Modeling,* MIT Press, Cambridge, MA, 1987
25. S. Wolfram, *A New Kind of Science,* Wolfram Media Inc, Champaign, IL, 2002
26. B. Chopard and M. Droz, *Cellular Automata Modeling of Physical Systems,* Cambridge University Press, Cambridge, UK, 1998
27. M. Rapapaz, and C.A. Gandin, Probabilistic Modeling of Microstructure Formation in Solidification Processes, *Acta Metall. Mater.,* Vol 41, 1993, p 345-360
28. J.A. Spittle and S.G.R. Brown, A 3d Cellular-Automaton Model of Coupled Growth in 2-Component Systems, *Acta Metall. Mater.,* Vol 42, 1994, p 1811-1815
29. N. Chakraborti, P. Mishra, and Ş. Erkoç, A Study of the Cu Clusters Using Gray-Coded Genetic Algorithms and Differential Evolution, *J. Phase Equlib. Diffusion,* Vol 25, 2003, p 16-21
30. N. Chakraborti, P. Mishra, and A. Banerjee, Optimization of Aluminum Oxynitride Compaction Process Using a Gray-Coded Genetic Algorithm, *Mater. Lett.,* Vol 58, 2004, p 136-141
31. J.W. Christian, *The Theory of Transformations in Metals and Alloys* (Part-I), Pergamon, Oxford, UK, 2002
32. K. Deb, A.R Reddy and G. Singh, Optimal Scheduling of Casting Sequence Using Genetic Algorithms, *Mater. Manufact. Proc.,* Vol 18**,** 2003, p 409-432
33. N. Chakraborti, Genetic Algorithms in Materials Design and Processing, *Int. Mater, Rev.,* Vol 49, 2004, p 246-260
34. D.D. Wang, A.K. Tieu, and G. D'Alessio, Computational Intelligence Based Process Optimization for Tandem Cold Rolling, *Mater. Manufact. Proc.,* Vol 20, 2005, p 479-496
35. R. Nandan, R. Rai, R. Jayakanth, S. Moitra, N. Chakraborti, and A. Mukhopadhyay, Regulating Crown and Flatness During Hot Rolling: A Multi-Objective Optimization Study Using Genetic Algorithms, *Mater. Manufact. Proc.,* Vol 20, 2005, p 459-478